IEEE Access
Multidisciplinary | Rapid Review | Open Access Journal

Received August 31, 2020, accepted September 12, 2020, date of publication September 18, 2020,
date of current version September 30, 2020.

Digital Object Identifier 10.1109/ACCESS.2020.3025085

Wire-Suspended Device Control Based on Wireless Communication With Multirotor for Long Reach-Aerial Manipulation

RYO MIYAZAKI, (Graduate Student Member, IEEE),
HANNIBAL PAUL, (Graduate Student Member, IEEE),
TAKAMASA KOMINAMI, (Graduate Student Member, IEEE),
AND KAZUHIRO SHIMONOMURA, (Member, IEEE)
Department of Robotics, Ritsumeikan University, Kusatsu 5258577, Japan

Corresponding authors: Ryo Miyazaki (rr0045vp@ed.ritsumei.ac.jp) and Kazuhiro Shimonomura (skazu@fc.ritsumei.ac.jp)

ABSTRACT In this study, we propose a long-reach aerial manipulation system with a wire-suspended device that allows the airframe to maintain its position at the desired distance away from the target. We implemented a feedback communication between the multirotor and wire-suspended device to maintain the position of the wire-suspended device directly below the multirotor while maintaining a constant distance from the target. The multirotor communicates its velocity and relative position to the wire-suspended device to control the ducted fans, whereas the wire-suspended device transmits the attitude and distance from the ground to the multirotor to control the winch. The designed controller for the ducted fans allows the wire-suspended device to behave like a long rigid robotic arm. The performance of the designed controller was verified by navigating the multirotor over stepped surfaces while the wire-suspended device was being lowered.

INDEX TERMS Unmanned aerial vehicles (UAV), long reach aerial manipulation, field robotics.

I. INTRODUCTION

Aerial manipulation via UAVs equipped with a robotic arm has been actively studied for several years [1]–[6]. This technology is useful in various dangerous activities, such as maintenance and inspection of high-voltage electric lines, windmill blades, bridges, dam walls, tunnel roofs, etc. In some previous aerial manipulation systems, the manipulator was designed compactly and attached to the bottom [1], [2], [4], side [5], or top [6] of the body frame. However, some applications require the work point to be away from the UAV body. For example, if the target is a lightweight object or something that is placed unstably, the effect of downwash [8], [9], i.e., the downward wind generated by the propellers, cannot be ignored. If the target is in a narrow region or cluttered environment, it is difficult to reach the target and manipulate it directly using a UAV. Additionally, for cooperating or establishing contact with humans in a search-and-rescue task [10], it is essential to maintain a safe distance.

The associate editor coordinating the review of this manuscript and approving it for publication was Ehsan Asadi.

For the afore-mentioned scenarios, a long-reach manipulator with a long-link robotic arm [11]–[13] and a manipulator with an origami structure [14] were proposed. The long-reach manipulators were designed with a maximum length of 1 – 1.5 m, which is insufficient for such situations. However, increasing the length of the manipulator may disturb the multirotor flight. Alternatively, this problem can be addressed by employing a winch mechanism and a wire-suspended hand. In some studies [15]–[17], cable-suspended aerial manipulators were simulated and developed using industrial manipulators and 8 thrusters for stabilizing the swinging motion. In our previous study [7], we developed a long and light wire-suspended hand. The wire-suspended hand consisted of four ducted fans with an IMU and robotic hands with a vision system. The IMU sensor with the ducted fans was used for suppressing the swinging motion of the wire-suspended hand within a distance of 3.5 m from the UAV.

However, while moving, suppressing the swinging motion can cause the wire-suspended hand to stay away from the required position directly below the UAV (FIGURE 1, without position control system). This happens because the swinging motion of the device is suppressed using IMU

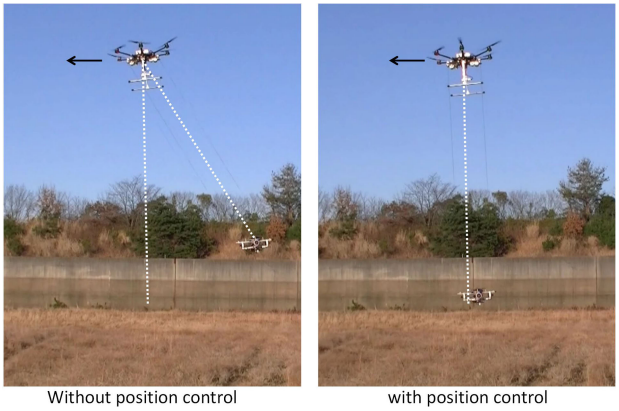

FIGURE 1. Various states of the wire-suspended device while flying (UAV was controlled to go left). The left figure shows the state of the wire-suspended device without using the position control system. The device was programmed for suppressing the swinging motion using sensor feedback [7]. Faster the UAV moves, more the misalignment between the UAV and wire-suspended device. The right figure shows the state of the device while using the position control system. The device can be controlled to stay directly below the UAV during the flight.

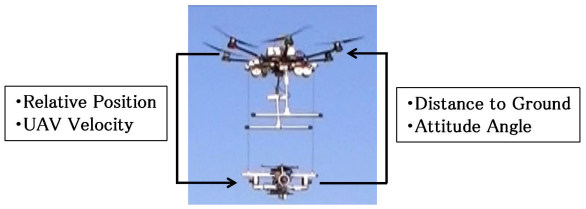

FIGURE 2. Communication between the wire-suspended device and multirotor.

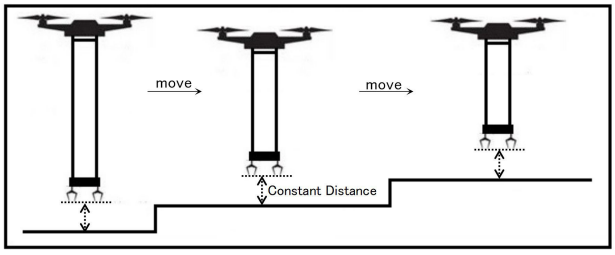

FIGURE 3. Testing scenario for the position control system of the wire-suspended device.

inputs only, which do not have any feedback regarding the UAV flight state and relative position of the UAV with respect to the wire-suspended device. The swinging motion (FIGURE 1, without position control system) not only reduces the speed of the UAV but also requires a longer time for the wire-suspended hand to reach the target. To improve the manipulation ability of the system and allow the UAV to move freely with respect to the wire-suspended hand, the inclination angle of the UAV should be small while moving (FIGURE 1, with position control system). Furthermore, the winch mechanism was placed on the UAV to reduce the weight of the wire-suspended device. To control the winch automatically, it requires sensor feedback from the wire-suspended device.

To overcome the afore-mentioned problems, we enabled the UAV and wire-suspended device to communicate between each other. Based on this communication link, we designed a position controller that can control the wire-suspended device to stay directly below the UAV (FIGURE 1, with position control system) during the flight. This allowed the device to behave like a rigid long-reach manipulator. Additionally, we developed an autonomous winch system to control the attitude of the wire-suspended device and maintain a constant distance from the ground.

The main purpose of this study is to develop a communication loop between the UAV and the wire-suspended device and design new controllers for the wire-suspended device and winch. Section II presents the main contribution of this study, including design concepts and scenarios. Section III discusses our previous work along with device and system customizations. Section IV discusses the sensing and control methods, and the indoor test, whereas Section V explains the first outdoor experimental results of the proposed system. Finally, Section VI concludes this paper by presenting the conclusions and future work.

II. INTERCOMMUNICATION FOR WIRE-SUSPENDED DEVICE CONTROL

In the pick-and-place task [7], we verified that it was possible to perform few manipulation tasks using the proposed method. However, the tasks were performed by moving the UAV slowly because quick UAV movements caused a position drift between the UAV and wire-suspended hand in the horizontal plane. Moreover, this limits the moving speed of the UAV and extends the working time. Nevertheless, these problems can be solved by transmitting the relative position and UAV velocity to the wire-suspended device. By integrating the received data, the ducted fans equipped on the wire-suspended device can provide optimized thrust for staying directly below the UAV during the flight. FIGURE 2 shows the concept of position control of the wire-suspended device based on the proposed communication technique with the multirotor.

In some UAV applications for industrial maintenance and inspection, the UAV needs to stay near the target point. In our experiment, we programmed the wire-suspended device to maintain a certain distance from the target to obtain high-accuracy data. However, we need to protect the device so that it never hits the target. Therefore, the winch had to be controlled automatically. This was achieved by transmitting the distance to the target surface and device attitude from the wire-suspended device to the UAV (FIGURE 2). Thus, the winch was able to control the wire-suspended device to stay horizontal and maintain a constant distance from the target surface during the flight. Moreover, the autonomous winch control system can also be used for avoiding obstacles around the wire-suspended hand in complex environments. The performance is much smoother than that by controlling UAV.

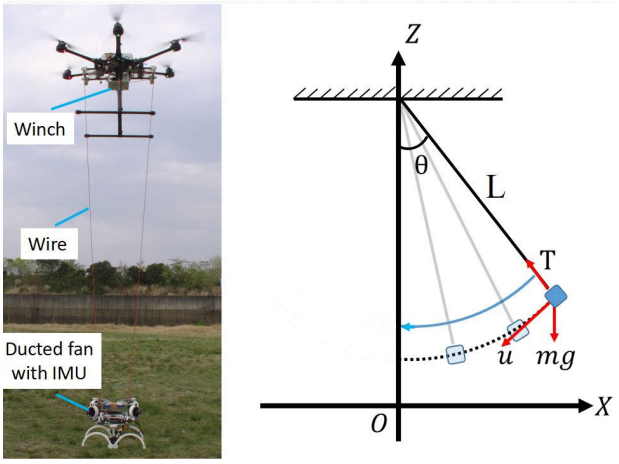

FIGURE 4. Aerial robot platform with the swinging model of the wire-suspended hand.

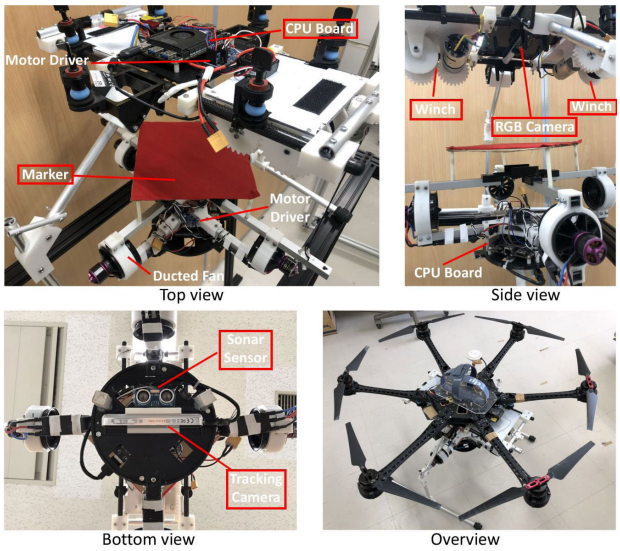

FIGURE 5. Main devices used in the UAV platform along with the wire-suspended device. The red square in the picture shows the newly installed device.

In this study, we considered a scenario, as shown in FIGURE 3. The long-reach manipulator (wire-suspended device with winch) behaved like a rigid robotic arm and maintained a constant distance during the flight. This quality can be helpful in industrial applications, such as inspection of high-voltage electric lines, solar panels, bridges, or search-and-rescue tasks that require the manipulator to be very close to the target while requiring the UAV to be at a safe distance away from the target.

III. SYSTEM

A. AERIAL ROBOT PLATFORM WITH SWING SUPPRESSION CONTROL

The aerial robot platform consists of a winch equipped UAV and a wire-suspended hand. The hand, which is suspended by two wires to avoid the twist motion, includes four ducted fans with an IMU for swing suppression and a robotic hand for aerial manipulation tasks. As shown in FIGURE 4, the swinging motion of the wire-suspended hand was assumed to be similar to that of a single pendulum, where an external opposing force u acting on the pendulum can stabilize the motion faster. The controller of the swing suppression can be given by:

$$u = -sgn(V)K_{rp}\theta - K_{rv}V \tag{1}$$

where K_{rp} and K_{rv} are the control gains, which were tuned based on the simulation and experiment. V is the linear velocity of the wire-suspended hand, which can be estimated from the IMU. The swing suppression control and pick-and-place task were demonstrated successfully in our previous study [7].

B. REDESIGNING DEVICE AND THE SYSTEM

We customized the UAV platform and wire-suspended device according to the proposed scenario (FIGURE 5). The UAV comprises of a hexarotor airframe (DJI S800, FIGURE 5, overview) that includes the flight controller (DJIN3), CPU board (LattePanda Alpha 864, which contains WiFi 802.11 ac module and Arduino Leonardo), RGB camera (Logicool C270n), motor driver (PCA9685), and dual winch mechanism (DC geared motor 540K75 with two 5 m long wires). The CPU board is used for communicating with the wire-suspended device, image processing, and winch control. To maintain the wire-suspended device horizontal while the UAV is moving, as shown in 3, the winch mechanism was redesigned from a single motor type in [7] to a dual motor type (FIGURE 5, side view). The motor driver receives I2C signals from the winch controller and converts it to PWM signals to control the rotational speed of the DC motor via the ESC.

The wire-suspended device consists of four ducted fans (Powerfun EDF 50 mm with 0.95 kg of maximum trust), ESC, motor driver (PCA9685), CPU board (LattePanda Alpha 864), tracking camera (RealSense T265, stereo fisheye camera with IMU), sonar sensor (HC-SR04), and a color marker. The CPU board is used for communicating with the UAV and position controller. The motor driver receives I2C signals from the position controller and converts them to PWM signals, which is received by the ESC to control the rotational speed of the DC motor (ducted fan). The tracking camera can provide velocity and attitude data for designing the position and winch controllers. In [7], the IMU was used for estimating the velocity to suppress the swinging motion. However, the result had poor accuracy owing to the low update rate (50 Hz). The tracking camera provides better accuracy at a higher rate (200 Hz) without any calculation costs on the CPU board. The sonar sensor is used for measuring the distance from the wire-suspended device to the ground.

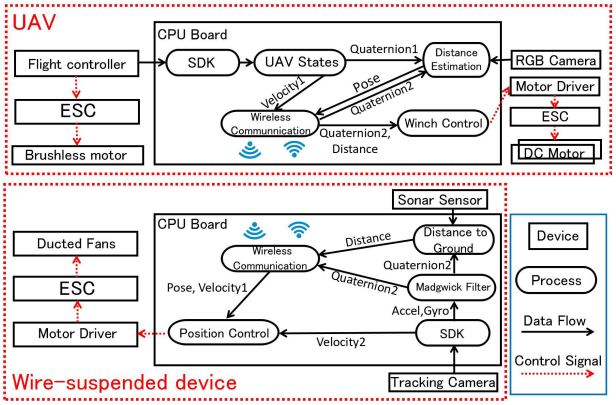

FIGURE 6. Block diagram of the UAV and wire-suspended device.

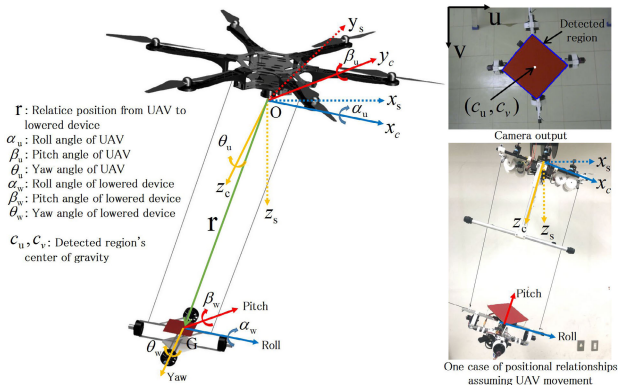

FIGURE 7. Coordinate configuration (left) and a case with positional relationships considering the UAV flight in side view (right bottom). The top right figure shows the output from the camera mounted on the UAV for the same case. In the camera image (top right), the blue line shows the detected region and the white point shows the center of gravity in that region.

FIGURE 6 shows the block diagram for the proposed system. The Wi-Fi module on the CPU board of the wire-suspended device was used as a hotspot to create an access point to connect the Wi-Fi modules on the UAV and wire-suspended device and establish communication between them. All sensor data were shared between the CPUs via the Robot Operating System. To analyze the communication delay in the system, we placed the UAV 5 m (maximum wire length) away from the wire-suspended device. The average communication delay was found to be 0.42 ms. For sensing, in the tracking camera, the velocity data based on camera coordination and IMU data (raw data of acceleration and gyro) from the SDK were used. The Madgwick filter [18] was used to calculate the quaternion (attitude) of the wire-suspended device from the acceleration and gyro data. The velocity data and quaternion was obtained from the flight controller of the UAV via the SDK. To estimate the relative position of the wire-suspended device with respect to the UAV, the RGB camera mounted on the UAV (FIGURE 5, side view) was used to detect the marker equipped on the wire-suspended device (FIGURE 5, top view). The coordination was then corrected by the calculated position using both the quaternions (Quaternion1 and 2 in FIGURE 6). The data from the sonar sensor was corrected using the quaternion (Quaternion 2) to correspond to small rolling of the wire-suspended device during flight while being lowered. For controlling the UAV, the position controller was designed using the velocity data (Velocity1 and 2 in FIGURE 6) along with relative position estimation, whereas the winch controller was designed using the quaternion (Quaternion 2) and corrected distance data (Distance in FIGURE 6).

IV. SENSING AND CONTROL

A. ESTIMATION OF RELATIVE POSITION AND DISTANCE

There are two methods to estimate the relative position between the UAV and wire-suspended device. In the first method, the wire length and inclination angle is measured, whereas a marker is visually tracked in the second method. However, the cumulative error in the first method increases with time due to the use of encoders to measure the wire length. Additionally, a small twist in the wire will affect the estimation result. In other words, the error will increase as the wire-suspended hand is lowered.

Therefore, visual tracking of the color marker and IMU sensor (included in tracking camera, FIGURE 5) were used for position estimation. The ArUco marker with a monocular camera can be another choice for calculating 6-DOF position and attitude. However, using the color marker and IMU has the following advantage in our scenario.

- *Detectable range*: According to the designed winch mechanism, the detectable range should be within 5 m. Therefore, the maximum size of the marker was chosen to be 0.18 m × 0.18 m, so that the marker is visible even when the wire-suspended device is stored on the UAV. When we compared the performance of the ArUco marker and color marker for the same marker size, the detectable range of the ArUco marker was 0 to 2.65 m, whereas the range of the color marker was 0 to 4.8 m.
- *IMU sensor*: The ArUco marker requires additional calculation cost for estimating 6-DOF position and attitude. However, the attitude can be obtained from the tracking camera without additional computation (FIGURE 6). Furthermore, the accuracy of the attitude angle from the IMU sensor is much higher than that of a single ArUco marker, and using multiple ArUco markers will limit the maximum detectable range.

The camera resolution and frame rate are 640 × 480 pixels and 30 fps, respectively. To detect the color marker, we used the inRange function of OpenCV in the HSV color space to detect the specific color range (FIGURE 7, camera output of blue line) and calculated image coordination of center of gravity (FIGURE 7, camera output of white point) in the detected region. In FIGURE 7, the top right figure shows the detection result and the bottom right figure shows the

positional relationships of the UAV and wire-suspended device at that time. According to the coordinate configuration and parameters shown in FIGURE 7 (left), the 3-DOF relative position based on camera coordination ${}^{c}r$ can be given by:

$$ {}^{c}r = \begin{bmatrix} {}^{c}p_x \\ {}^{c}p_y \\ {}^{c}p_z \end{bmatrix} = \begin{bmatrix} \frac{(c_v - c_{vd})}{{}^{c}p_z f} \\ \frac{(c_u - c_{ud})}{{}^{c}p_z f} \\ f\sqrt{\frac{s\cos(\alpha_w)\cos(\beta_w)}{s'}} \end{bmatrix} \tag{2} $$

where c_{ud} and c_{vd} are the image center coordination. f is the focal length of the camera, and s and s' are the marker area of the real image (0.18 m × 0.18 m) and pixels in the image. The roll angle α_w and pitch angle β_w of the wire-suspended device are converted from the quaternion(Quaternion2 in FIGURE 6) and calculated for correcting the marker area in the image while the wire-suspended device is being inclined. To position the wire-suspended device directly under the UAV, the relative position should be based on the horizontal surface of the UAV(FIGURE 7, bottom left and right). The converted relative position ${}^{s}r$ can be calculated by:

$$ {}^{s}r = \begin{bmatrix} {}^{s}p_x \\ {}^{s}p_y \\ {}^{s}p_z \end{bmatrix} = {}^{s}R_x(-\alpha_u){}^{s}R_y(-\beta_u){}^{c}r \tag{3} $$

where, ${}^{s}R_x$ and ${}^{s}R_y$ are the rotation matrices of the UAV about its roll and pitch axes, respectively. The roll angle α_u and pitch angle β_u of the UAV can be converted from the quaternion (Quaternion1 in FIGURE 6). Whereas, between the wire-suspended device and ground can be calculated from the sonar feedback using the roll and pitch angle of the wire-suspended device, which is given by:

$$ d_{fix} = d_{raw}\cos(\alpha_w)\cos(\beta_w) \tag{4} $$

where d_{fix} and d_{raw} are the corrected vertical distance and raw distance data from the sonar sensor, respectively.

B. DEVICE CONTROLLERS

In this study, we assume that the UAV moves mainly along the X_s direction (FIGURES 7 and 8 (left)). When the UAV needs to change the heading direction, the yaw axis of the UAV can be controlled. The model of the system in the X_s-Z_s plane is shown in FIGURE 7 (left). The motion equation of the wire-suspended device motion is given by:

$$ m\ddot{x} = mg\frac{x}{l} - k\dot{x} + u \tag{5} $$

where the viscosity coefficient k, whose value was calculated in our previous research [7], is the parameter corresponding to air resistance or friction. The wire length l can be calculated from the variables in Equation (1) as shown below:

$$ l = \sqrt{{}^{c}p_x^2 + {}^{c}p_y^2 + {}^{c}p_z^2} \tag{6} $$

According to Equation (5), the state equation is given by:

$$ \dot{x} = Ax + Bu \tag{7} $$

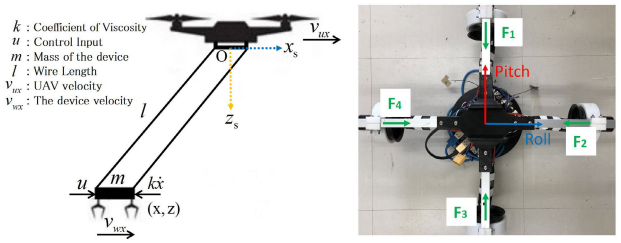

FIGURE 8. Model of the wire-suspended device with the UAV (left). The coordination was set similar to that in FIGURE 7. The right figure shows the arrangement of ducted fans that generate the force (F_1, F_2, F_3 and F_4, respectively) for position control and swing suppression. The direction of roll and pitch axes are same as that shown in FIGURE 7.

where $x = [x\ \dot{x}]^T$, with

$$ A = \begin{bmatrix} 0 & 1 \\ \frac{g}{l} & -\frac{k}{m} \end{bmatrix}, B = \begin{bmatrix} 0 \\ \frac{1}{m} \end{bmatrix} \tag{8} $$

The controller was designed using the stationary LQR technique. Furthermore, the MATLAB library was used to calculate the state feedback gain and tune the appropriate metrics Q and R, which are given by:

$$ Q = \begin{bmatrix} 1 & 0 \\ 0 & 10 \end{bmatrix}, R = \begin{bmatrix} 1 \end{bmatrix}, \tag{9} $$

The control gain was programmed to calculate every time before controlling, because the wire length l was changed by the winch control system in metrics A. According to Equation (5) - (9) and the parameters shown in FIGURE 8, the control input along the roll axis can be given as follows:

$$ u_{roll} = K_1{}^{s}p_x + K_2(v_{ux} - v_{wx}) \tag{10} $$

The velocity of the UAV v_{ux} and wire-suspended device v_{wx} can be obtained from the UAV flight controller of UAV and tracking camera, respectively (FIGURE 6, Velocity1 and Velocity2). Swing suppression control is used as the control input along the pitch axis, which is similar to Equation (1) and is given by:

$$ u_{pitch} = -K_s v_{wy} \tag{11} $$

where K_s is the control gain of the swing suppression. Finally, the control input for the ducted fan(FIGURE 8, right) is given by:

$$ u_{fans} = \begin{bmatrix} u_1 \\ u_2 \\ u_3 \\ u_4 \end{bmatrix} = \begin{bmatrix} -\nu u_{pitch} + \xi \\ -\nu u_{roll} + \xi \\ \nu u_{pitch} + \xi \\ \nu u_{roll} + \xi \end{bmatrix} \tag{12} $$

$$ \begin{aligned} u_1 = 0(u_{pitch} > 0)\ u_2 = 0(u_{roll} > 0) \\ u_3 = 0(u_{pitch} < 0)\ u_4 = 0(u_{roll} < 0) \end{aligned} \tag{13} $$

In Equation (12), ν and ξ are the parameters for converting the control input value to the PWM signal.

For the winch control, the PD controller was used for attitude and distance control, which can be given by:

$$ \begin{cases} u_{att} = -K_{aP}\alpha_w - K_{aD}\dot{\alpha_w} \\ u_{dis} = K_{dP}d_{err} + K_{dD}\dot{d_{err}} \end{cases} \tag{14} $$

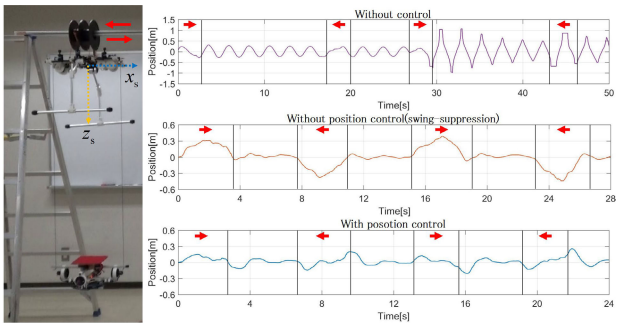

FIGURE 9. Experimental setup (left) and results (right). The UAV was fixed to move only along the X_S axis. The experimental results (right) shows the relative position of the wire-suspended device with respect to the UAV on the X_S axis. The experiment was conducted for the case of no-control (top right), without position control system (swing suppression control, center right) and with position control system (bottom right). The blocked region containing the red arrow shows the direction in which the UAV flew.

where u_{att}, u_{dis}, K_{aP}, K_{aD}, K_{dP} and K_{dD} are the control inputs and gains for the attitude controller and distance controllers. d_{err} is the error in distance, which can be calculated using Equation (4). Referring to the equation, the control input for the motors in the winch can be given by:

$$\begin{cases} u_{m1} = u_{att} + u_{v2} \\ u_{m2} = u_{dis} \end{cases} \tag{15}$$

The motor on the right side is numbered as 1 and that on the left side as 2, as shown in 7. One motor is used to control the wire length and the other motor is used to stabilize the attitude of the wire-suspended hand. To smoothen the winch control mechanism u_{v2} was added (corresponding to the rotational speed of motor 2) in motor 1, which controls the attitude. The attitude control allows the wire-suspended hand to stay horizontal to minimize the output of the ducted fans. Additionally, it can be used for controlling the attitude of the wire-suspended hand during manipulation.

C. INDOOR TEST OF THE SYSTEM

To verify the designed systems, the position and winch control systems were tested experimentally. The setup for the position control experiment is shown in FIGURE 9. The UAV was fixed on the top and flown along the X_s direction. The wire length was set to be 1.5 m. To verify the effectiveness of the designed position control system, we repeated the experiment without using the position control system (i.e., swing suppression control only, same control input from Equation (11)) and in the case of no-control. The behavior of the wire-suspended device while the UAV was moving was demonstrated in the experiments. The results are shown in FIGURE 9. In the case of no-control (FIGURE 9, top right), the relative position offset was observed to be large while the UAV was moving. Moreover, the wire-suspended device started swinging when the UAV was stopped. In the swing suppression control case (FIGURE 9, center right), the relative maximum position was observed to be approximately 0.3 m when the UAV was moving. When the position control system was used, the relative position offset was observed to be within 0.15 m even when the UAV started or stopped moving immediately. Nevertheless, the position error was reduced and the device was positioned directly below the UAV within 0.05 m. Similar results were obtained even when the experiment was repeated several times.

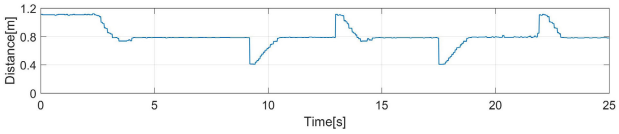

FIGURE 10. Indoor experimental result of the winch control system. The graph shows the distance between the wire-suspended device and ground. The target distance was set to be 0.8 m.

The setup shown in FIGURE 9 was also used to perform the winch control experiment. Firstly, the wire-suspended device was winched up such that it was right below the UAV and started the control. The target distance was set as 0.8 m. The experimental result is shown in FIGURE 10. In the graph, the device was controlled to reach to the target distance(in FIGURE 10, the time is approximately 4 s). In the following stage, we inserted and removed a 0.4 m box twice under the device to check the performance of the winch. According to the experimental results, for the 0.4 m error in distance, it took 1 s to reach the target and approximately 0.02 m error remained. The winch was controlled with high precision, which required additional convergence time.

V. FLIGHT EXPERIMENTS

To verify the developed system and controller while the UAV is flying, we performed three experiments. The first experiment was conducted for testing the winch control system. The second experiment verified the effectiveness of the position control system. Finally, the third experiment was performed to verify whether the winch and position control systems can work without interfering with each other. The UAV was controlled manually in each experiment.

A. EXPERIMENT FOR TESTING THE WINCH CONTROL SYSTEM WHILE FLYING

The experimental set up is shown in FIGURE 11. The winch was used to control the height of the wire-suspended device and maintain a constant distance from the ground. The experiment started when the UAV was several meters above the ground and the wire-suspended device was lowered. To avoid the wire-suspended device from swinging, the swing suppression control mode was used. The UAV was flown up and down continuously after switching on the winch control system. The target distance from the wire-suspended device to the ground was set as 0.6 m. The experimental result is shown in FIGURE 11 (right). The top right graph shows the distance (corrected sonar sensor value in Equation (4)) and the bottom right graph shows the pitch angle of the wire-suspended device.

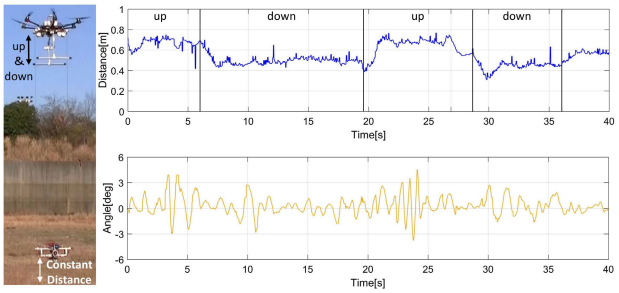

FIGURE 11. Experimental setup and result. The graph shows the distance between the wire-suspended device and ground (top right) and the pitch angle of the device. The target (constant) distance was set as 0.6 m.

The result demonstrates that a steady state error of approximately 0.1 m was observed while the UAV went up and down continuously. This was caused due to the unsteady UAV motion and slow convergence time of the winch. The device reached the target distance when the UAV started hovering (FIGURE 11, top right). The performance of the winch control system was similar to that in the indoor test. A small noise is visible in the graph because of the presence of grass on the ground. However, it did not affect the performance of the winch control system. As shown in FIGURE 11 (bottom right), the pitch angle was controlled in the range of ± 3 degree so that the device was able to stay horizontal during the flight. From this experiment, we verified that the autonomous winch control system works without affecting the flight of the UAV. However, the UAV motion (up and down) affects the performance of the winch control system.

B. EXPERIMENT FOR TESTING THE POSITION CONTROL SYSTEM WHILE FLYING

To perform this experiment, the UAV was positioned approximately 5 m above the ground and the wire-suspended device was lowered by 3 m from the UAV. During the experiment, the UAV moved at a relatively high speed of approximately 8 m/s (momentary maximum speed) along the X_s axis. The experiment was performed twice, i.e., with and without the position control system of the wire-suspended device. To compare the difference between the two trials, the UAV was navigated along the same route at the same speed.

The continuous images captured with and without the position control system during the flight are shown in FIGURE 12. When the position control system was used (FIGURE 12, top four images), the wire-suspended device was observed to be directly under the UAV. Whereas, in the other case (FIGURE 12, bottom four images), the relative position of the wire-suspended device with respect to the UAV along the X_s axis was highly instable during the flight. Moreover, the device went beyond the view of the camera mounted under the UAV. The experimental results in FIGURE 13 show the relative position of the wire-suspended device with respect to the UAV (calculated using Equation (3)). The top and bottom graphs show the experimental results with and without the position control system while

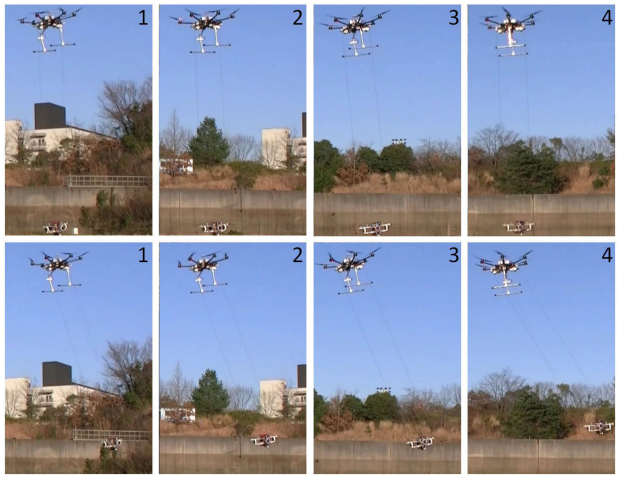

FIGURE 12. Continuous images of position control system (top four pictures) and without position control (swing suppression control, bottom four pictures) during flight. The order of top and bottom pictures is from 1 to 4.

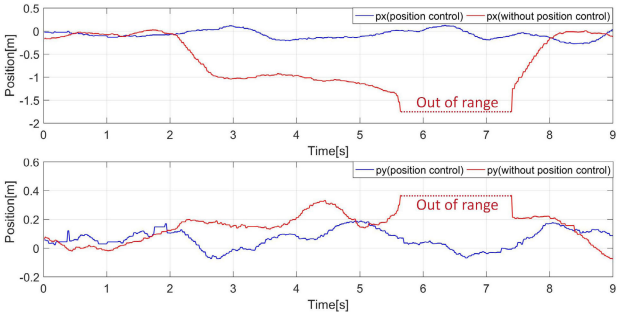

FIGURE 13. Experimental results showing the performance of the wire-suspended hand with and without the position control system. These graphs show the relative position of the UAV and wire-suspended device along the X_S axis (top graph) and Y_S axis (bottom graph) in FIGURE 7.

moving along the X_s and Y_s axes. According to the result along the X_s axis (FIGURE 13, top), for a 3 m length of wire, the wire-suspended device was positioned within an error of ± 0.1 m during the flight while using the position control system. Whereas, this error was approximately 1.5 m (maximum displacement) when the position control system was not used. The experimental result along the Y_s axis (FIGURE 13, bottom) was similar in both the scenarios. However, the out-of-range zone was observed when the position control system was not used. Therefore, this experiment verifies the effectiveness of the designed controller. The wire-suspended device required less than half the time to become stable from a big swing. Moreover, the swing suppression control (i.e., without position control system) also performed better compared to that in our previous study [7].

C. EXPERIMENT FOR TESTING INDEPENDENCE OF POSITION AND WINCH CONTROL SYSTEMS WHILE FLYING

To verify whether the winch and position control systems can work simultaneously without interfering with each other and if it is possible to realize the scenario shown in 3,

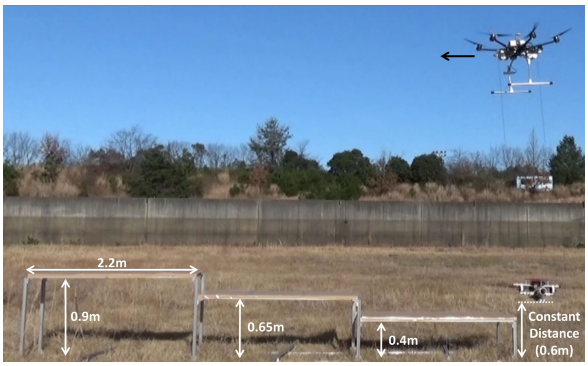

FIGURE 14. Experimental setup for the winch and position control systems. In the winch control experiment, the target (constant) distance from the wire-suspended device to the ground surface was set to be 0.6 m. The UAV height was kept constant while flying sideways (from left to right) to pass over a stepped surface.

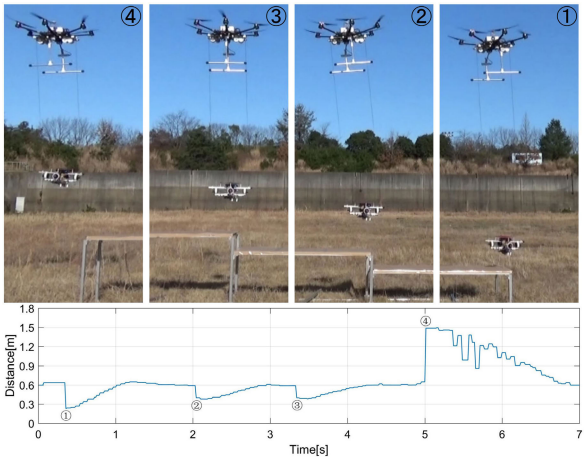

FIGURE 15. Continuous images (top) and experimental result showing the distance from the wire-suspended device to the ground (bottom). The value shown in the graph is the calculation result of Equation (3). The process follows ① to ④ and corresponds to the same number in the graph bottom.

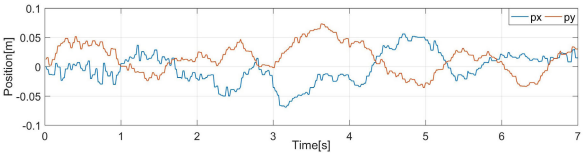

FIGURE 16. Outdoor experimental result of the position control system. The graph shows the relative position of the wire-suspended device with respect to the UAV along the X_S and Y_S axes(FIGURE 7).

the experiment was conducted, as shown in FIGURE 14. The UAV was flown sideways (left to right side) at a constant height while the winch automatically controlled the wire-suspended device to pass over the steps by maintaining a constant distance between the device and the surface while using the position control system.

The continuous images captured during the experiment are shown in FIGURE 15 (top). In this experiment, the winch and wire-suspended device worked smoothly to successfully pass over the stepped surface. The experimental results are shown in FIGURE 15 (bottom) and FIGURE 16. In FIGURE 15, the number in the graph indicates when the distance between the wire-suspended device and ground changed. The winch was controlled within a steady state error of 0.02 m and took approximately 1 s to reach the target distance. The accuracy of the winch control system was almost similar to that in indoor test (FIGURE 10) and higher than the experimental result as shown in FIGURE 11. In FIGURE 16, the graph shows the relative position of the lowered wire-suspended device with respect to the UAV along the X_s and Y_s axis. The wire-suspended device was maintained within a positioning error of ± 0.06 m. The experiment was repeated five times and each trial showed similar results.

From this experiment, we verified that the winch and position control systems worked as expected without affecting the flight of the UAV. Moreover, it can be easy to realize the application of avoiding obstacles by changing the sensor direction from the wire-suspended device.

VI. CONCLUSION

In this study, we proposed a position control system for the wire-suspended device that communicates with the UAV. The main contribution of this study is described as follows:

- The UAV and wire-suspended device system were developed based on wireless communication for long-reach aerial manipulation.
- The winch controller on the UAV system was designed using sensor feedback from the wire-suspended hand. This allows the winch to control the distance between the wire-suspended device and ground.
- The position controller on the wire-suspended device was designed using sensor feedback from the UAV. This allows the wire-suspended device to maintain its position directly below the UAV and behave as a rigid long-reach manipulator.

Through experiments, we show the autonomous winch control and position control of the wire suspended device to verify that all of system worked as expected.

In future work, estimating the relative position of the wire-suspended hand with respect to the UAV by visually tracking the red marker can fail in several situations (e.g., low visibility, objects in the scene with similar color, etc.). We plan to address this drawback by employing an RGBD camera with an LED marker array. Furthermore, the use of two wires to avoid the rotating motion of the wire-suspended hand causes it to roll along the X_s axis. The dual winch system is inadequate to control the 2-DOF attitude of the wire-suspended hand. Moreover, the convergence time of the winch system cannot be ignored for improving the manipulation efficiency. To overcome these problems, the winch system needs to be improved for a shorter convergence time. The use of additional wires to suspend the device can help in avoiding the rolling motion. Furthermore, we plan to

achieve long-reach manipulation with higher precision via autonomous localization by improving the proposed system.

REFERENCES

[1] D. Mellinger, Q. Lindsey, M. Shomin, and V. Kumar, "Design, modeling, estimation and control for aerial grasping and manipulation," in *Proc. IEEE/RSJ Int. Conf. Intell. Robots Syst.*, Sep. 2011, pp. 2668–2673.
[2] F. Huber, K. Kondak, K. Krieger, D. Sommer, M. Schwarzbach, M. Laiacker, I. Kossyk, S. Parusel, S. Haddadin, and A. Albu-Schaffer, "First analysis and experiments in aerial manipulation using fully actuated redundant robot arm," in *Proc. IEEE/RSJ Int. Conf. Intell. Robots Syst.*, Nov. 2013, pp. 3452–3457.
[3] F. Ruggiero, V. Lippiello, and A. Ollero, "Aerial manipulation: A literature review," *IEEE Robot. Autom. Lett.*, vol. 3, no. 3, pp. 1957–1964, Jul. 2018.
[4] F. Ruggiero, M. A. Trujillo, R. Cano, H. Ascorbe, A. Viguria, C. Perez, V. Lippiello, A. Ollero, and B. Siciliano, "A multilayer control for multirotor UAVs equipped with a servo robot arm," in *Proc. IEEE Int. Conf. Robot. Autom. (ICRA)*, May 2015, pp. 4014–4020.
[5] M. Fumagalli, R. Naldi, A. Macchelli, R. Carloni, S. Stramigioli, and L. Marconi, "Modeling and control of a flying robot for contact inspection," in *Proc. IEEE/RSJ Int. Conf. Intell. Robots Syst.*, Oct. 2012, pp. 3532–3537.
[6] J. Thomas, G. Loianno, K. Daniilidis, and V. Kumar, "Visual servoing of quadrotors for perching by hanging from cylindrical objects," *IEEE Robot. Autom. Lett.*, vol. 1, no. 1, pp. 57–64, Jan. 2016.
[7] R. Miyazaki, R. Jiang, H. Paul, Y. Huang, and K. Shimonomura, "Long-reach aerial manipulation employing wire-suspended hand with swing-suppression device," *IEEE Robot. Autom. Lett.*, vol. 4, no. 3, pp. 3045–3052, Jul. 2019.
[8] D. Yeo, E. Shrestha, D. A. Paley, and E. M. Atkins, "An empirical model of rotorcrafy UAV downwash for disturbance localization and avoidance," in *Proc. AIAA Atmos. Flight Mech. Conf.*, Jan. 2015, p. 1685.
[9] R. Miyazaki, R. Jiang, H. Paul, K. Ono, and K. Shimonomura, "Airborne docking for multi-rotor aerial manipulation," in *Proc. IEEE/RSJ Int. Conf. Intell. Robots Syst. (IROS)*, Oct. 2018, pp. 4708–4714.
[10] J. M. Gomez-de-Gabriel, J. M. Gandarias, F. J. Perez-Maldonado, F. J. Garcia-Nuncz, E. J. Fernandez-Garcia, and A. J. Garcia-Cerezo, "Methods for autonomous wristband placement with a search-and-rescue aerial manipulator," in *Proc. IEEE/RSJ Int. Conf. Intell. Robots Syst. (IROS)*, Oct. 2018, pp. 7838–7844.
[11] A. Caballero, A. Suarez, F. Real, V. M. Vega, M. Bejar, A. Rodriguez-Castano, and A. Ollero, "First experimental results on motion planning for transportation in aerial long-reach manipulators with two arms," in *Proc. IEEE/RSJ Int. Conf. Intell. Robots Syst. (IROS)*, Oct. 2018, pp. 8471–8477.
[12] A. Suarez, P. Sanchez-Cuevas, M. Fernandez, M. Perez, G. Heredia, and A. Ollero, "Lightweight and compliant long reach aerial manipulator for inspection operations," in *Proc. IEEE/RSJ Int. Conf. Intell. Robots Syst. (IROS)*, Oct. 2018, pp. 6742–6746.
[13] A. Suarez, F. Real, V. M. Vega, G. Heredia, A. Rodriguez-Castano, and A. Ollero, "Compliant bimanual aerial manipulation: Standard and long reach configurations," *IEEE Access*, vol. 8, pp. 88844–88865, 2020.
[14] S.-J. Kim, D.-Y. Lee, G.-P. Jung, and K.-J. Cho, "An origami-inspired, self-locking robotic arm that can be folded flat," *Sci. Robot.*, vol. 3, no. 16, Mar. 2018, Art. no. eaar2915.
[15] M. J. Kim, J. Lin, K. Kondak, D. Lee, and C. Ott, "Oscillation damping control of pendulum-like manipulation platform using moving masses," *IFAC-PapersOnLine*, vol. 51, no. 22, pp. 465–470, 2018.
[16] Y. S. Sarkisov, M. J. Kim, D. Bicego, D. Tsetserukou, C. Ott, A. Franchi, and K. Kondak, "Development of SAM: Cable-suspended aerial manipulator," in *Proc. Int. Conf. Robot. Autom. (ICRA)*, May 2019, pp. 5323–5329.
[17] Y. S. Sarkisov, M. Jun Kim, A. Coelho, D. Tsetserukou, C. Ott, and K. Kondak, "Optimal oscillation damping control of cable-suspended aerial manipulator with a single IMU sensor," 2020, *arXiv:2003.00472*. [Online]. Available: http://arxiv.org/abs/2003.00472
[18] S. Madgwick, "An efficient orientation filter for inertial and inertial/magnetic sensor arrays," Rep. x-io, Univ. Bristol, Bristol, U.K., Tech. Rep., 2010.

RYO MIYAZAKI (Graduate Student Member, IEEE) received the B.E. and master's degrees in mechanical engineering from Ritsumeikan University, Japan, in 2017 and 2019, respectively, where he is currently pursuing the Ph.D. degree. His research interests include designing long reach aerial manipulators, development of control systems with sensor fusion, and onboard vision system for unmanned aerial vehicle. His research was chosen as one of the finalists for IROS2018 Best Paper Award.

HANNIBAL PAUL (Graduate Student Member, IEEE) received the Diploma degree in electronics and communication engineering from Nitte Rukmini Adyanthaya Memorial Polytechnic, India, in 2012, and the B.E. degree in electronics and communication engineering and the master's degree in V.L.S.I. design and embedded systems from the Nitte Mahalinga Adyanthaya Memorial Institute of Technology, India, in 2015 and 2017, respectively. He is currently pursuing the Ph.D. degree with Ritsumeikan University, Japan. His research interests include designing of manipulator systems and sensing technologies for unmanned aerial manipulation. He received the AIM-Machines Best Paper Award, in 2018. His research was also a finalist for IROS2019 Best Paper Award on safety, security, and rescue robotics.

TAKAMASA KOMINAMI (Graduate Student Member, IEEE) received the B.E. degree in mechanical engineering from Ritsumeikan University, Japan, in 2018, where he is currently pursuing the master's degree. His research interests include designing of aerial robot, simultaneous localization and mapping (SLAM), and aerial manipulation with focus on unmanned aerial vehicle.

KAZUHIRO SHIMONOMURA (Member, IEEE) received the Ph.D. degree in electronic engineering from Osaka University, Osaka, Japan, in 2004. Following his study as a Postdoctoral Fellow and an Assistant Professor with Osaka University, he joined the Department of Robotics, Ritsumeikan University, as an Associate Professor, in 2009, and was promoted to a Professor, in 2018. He is currently a Professor with the Department of Robotics, Ritsumeikan University. His research interests include development of vision sensors and vision-based systems for intelligent robots. His current research projects include an aerial robot for manipulation tasks, a high-resolution tactile sensor using camera, an embedded computer vision, and an ultra-high-speed imaging.